Research Square

Preprints are preliminary reports that have not undergone peer review.
They should not be considered conclusive, used to inform clinical practice,
or referenced by the media as validated information.

Food waste-derived organic fertilizer drives uranium phytoextraction through synergistic coupling of phosphorus-mediated detoxification and microbial mobilization

Xiaoyan Wu
University of South China
Jian Liu
University of South China
Yingxuan Ouyang
University of South China
Zhijun Zhang
University of South China
Guicheng He
University of South China
Lingling Wu
University of South China
Dandan Zhang
Weifang University of Science and Technology
Pubo Chen
Peking University
Qiaohong Chen
Qidong Fengsu Drilling Tools Co., Ltd
Huang Yu
yuhuang@usc.edu.cn

University of South China

Research Article

Keywords: Food waste organic fertilizer, Uranium, Rhizosphere microbiome, Vetiveria zizanioides, Phytoremediation

Posted Date: November 26th, 2026

DOI: https://doi.org/10.21203/rs.3.rs-11777313/v1

License: This work is licensed under a Creative Commons Attribution 4.0 International License.
Read Full License

Additional Declarations: No competing interests reported.

Abstract

Phytoremediation of uranium (U)-contaminated soil is fundamentally constrained by the inherently low bioavailability of U and its severe phytotoxicity. Food waste-derived organic fertilizer (FOF) holds promise for regulating heavy metal behavior, yet its role in enhancing U phytoextraction remains unclear. This study investigated the effects of FOF, inorganic fertilizer (IF), and sheep manure organic fertilizer (SOF) on *Vetiveria zizanioides* phytoremediation of U-contaminated soil. Results showed that the optimal treatment ($FOF_{0.6}$+$IF_{0.4}$) removed 64.67% of U from soil, increased available phosphorus (AP) to 290.48 mg kg^{-1}, and boosted U accumulation by 218.6% in plant tissues, significantly outperforming IF and SOF treatments. FOF reshaped the rhizosphere microbiome by enriching plant growth-promoting *Pseudomonas*, U(VI)-detoxifying *Sphingomonas*, and inorganic P-solubilizing *Gemmatimonas*. Critically, metagenomic profiling revealed that, unlike SOF which stimulated U-reduction and immobilization, FOF suppressed reductive pathways but dramatically enriched heavy metal resistance and efflux genes (*azr*), establishing a conducive microenvironment that favored root proliferation. Structural equation modeling further revealed a synergistic coupling: P mineralization concurrently provided bioavailable P for plant growth and precipitated U in situ, while microbial metal metabolism and N cycling mobilized U from soil solids into the rhizosphere solution for plant uptake. Collectively, FOF drives U phytoextraction through a functional synergy: P-mediated detoxification establishes a low-stress niche for root growth, while microbial metal metabolism and N cycling actively mobilize U for continuous uptake. This study provides a novel mechanistic framework linking organic amendment-driven microbial nutrient cycling to pollutant fate in the rhizosphere, highlighting food waste valorization for improving soil fertility and bioremediation.

1. Introduction

Uranium (U), as a key strategic resource for the development of nuclear energy, has witnessed continuously growing supply and demand (Chandwadkar et al., 2023; Wu et al., 2023). Nevertheless, historical mining and metallurgical activities have left a severe legacy of soil contamination (Chen et al., 2022). The average U concentration in soils surrounding U mining has reached 103.7 mg kg^{-1}, which is approximately 40 times higher than that in the earth's crust (Cui et al., 2023). Due to its strong chemical toxicity and radioactivity, U in soil poses significant risks to regional ecological security and public health (Wang et al., 2023). Phytoremediation, particularly phytoextraction, is considered an economically viable and environmentally friendly strategy for remediating large areas of moderately contaminated soils (Islam et al., 2024). This technology leverages the biological processes of plants to volatilize, immobilize, filter, degrade, or extract pollutants (Peters et al., 2021; Xiong et al., 2025). However, the practical application of this technology is fundamentally constrained by two major bottlenecks: 1) the low bioavailability of U in the rhizosphere, wherein U in soil is readily immobilized by iron-manganese oxides or carbonate minerals, resulting in extremely low bioavailability content and hindering direct plant uptake (Akash et al., 2022; Edayilam et al., 2020); 2) plants struggle to colonize and survive in U-contaminated

soils, as uranyl ion (UO_2^{2+}) exhibit strong phytotoxicity, inhibiting root growth and inducing oxidative damage (Zheng et al., 2025; Muhammad et al., 2024).

To address these challenges, current remediation strategies predominantly target individual processes (e.g., either heavy metal mobilization or plant growth promotion) (Haneklaus et al., 2024; Yuan et al., 2024), while overlook the dynamic interactions among the rhizosphere chemical environment, microbial function traits, and plant responses. Thus, developing an eco-friendly approach capable of simultaneously realizing soil amelioration, U mobilization, and U-induced phytotoxicity is essential for enhancing the phytoremediation of U-contaminated soils. Inorganic fertilizers (IF) are widely utilized to stimulate plant biomass during phytoremediation, yet they fall short in ameliorating soil structure or mobilizing recalcitrant heavy metals (Fang et al., 2023). Traditional organic amendments, such as sheep manure organic fertilizer (SOF), are widely used to enhance soil fertility. However, previous studies indicate that SOF often promotes the formation of stable complexes or drives reducing microenvironments, leading to the reductive immobilization of heavy metals (Abreu et al., 2014). For a phytoextraction strategy, this immobilization is counterproductive because it reduces the pool of U available for root uptake. Therefore, there is an urgent need to identify alternative amendments that can simultaneously alleviate U phytotoxicity and maintain high U bioavailability.

Food waste-derived organic fertilizer (FOF) has recently attracted attention due to its high content of readily degradable organic matter and essential nutrients (Suvendran et al., 2025). Unlike traditional mature composts, FOF releases abundant dissolved organic matter (DOM) and small molecular organic acids during decomposition, which possess a strong capacity to regulate heavy metal behavior (Yassine et al., 2025). For instance, Yu et al. (2021) demonstrated that FOF significantly increased soil dissolved organic matter (DOM), which facilitated Cd transformation from residual fractions to bioavailable forms through complexation, thereby favoring subsequent phytoextraction. Zhao et al. (2023) further revealed that oxygen- and carbon-rich DOM compounds (e.g., polyphenols and carboxylic acids) selectively complex with Cd and Cu, demonstrating how key functional components in organic fertilizers drive heavy metal activation. In a 27-year field trial, Hussain et al. (2021) observed that organic fertilizer reduced soil pH and promoted Fe-Mn oxide dissolution, thereby enhancing Cd bioavailability. While these studies confirm FOF's effectiveness in mobilizing cationic heavy metals (e.g., Cd^{2+}, Pb^{2+}, Cu^{2+}, Zn^{2+}), whether FOF exerts similar mobilizing effects on U, a redox-sensitive metalloid, remains poorly understood. Furthermore, the underlying biological mechanisms by which FOF influences the rhizosphere microenvironment and the functional traits of the soil microbiome during U phytoextraction are largely unexplored.

The biogeochemical fate of U in the rhizosphere is highly complex, as its chemical speciation and bioavailability are predominantly governed by key edaphic factors including pH, redox potential, and organic matter content (Jun et al., 2025). In acidic soil, the bioavailability of U was significantly enhanced, thereby facilitating its uptake by plants (Yang et al., 2023). In oxidizing conditions, UO_2^{2+} forms highly mobile compounds, whereas U(VI) can be transformed into stable UO_2 under reducing

conditions (Huang et al., 2024). Humic acid can form complexes with UO_2^{2+} in solution due to its electronegativity, thereby increasing the mobility of U (Edayilam et al., 2020). Furthermore, rhizosphere microorganisms can mediate U mobilization by excreting organic acids or catalyzing Fe(III) reduction, while others can alleviate U toxicity through extracellular sequestration or metal efflux systems (Chi et al., 2023; Zhu et al., 2026). Microbial phosphorus (P) mineralization can generate free phosphate ions, which not only serve as essential nutrients for plant growth but also react with uranyl ions to form U-phosphate precipitates (Abdelkrim et al., 2020). However, we hypothesize that in the FOF-amended rhizosphere, it functions as a localized detoxification mechanism shielding the root apex from U phytotoxicity. Unlike the whole-scale reductive immobilization driven by SOF, FOF likely stimulates a distinct functional partitioning within the microbial community. Specifically, localized P mineralization acts as a frontline detoxification mechanism to protect root tips, while specific taxa drive metal and N cycling to maintain a bioavailable U(VI) pool for continuous plant uptake.

To test this hypothesis, a pot experiment was conducted using U-contaminated soil (178 mg kg^{-1}) collected from a representative mining site. We evaluated the effects of IF, SOF, FOF, and various combined application ratios on the growth of *Vetiveria zizanioides* (*V. zizanioides*) and U accumulation. By integrating soil physicochemical analysis, amplicon sequencing, metagenomic profiling, and structural equation modeling (SEM), this study aims to elucidate how FOF restructures the rhizosphere microbial community and its functional gene profiles to drive U phytoextraction. The findings are expected to provide a novel mechanistic framework for the sustainable valorization of food waste and the remediation of nuclear-contaminated environments.

2. Materials and methods

2.1. Soil collection, fertilizer preparation, and pot experiment design

Hengyang 272 mine (26°48'36"N, 112°40'12"E) is the first large-scale U hydrometallurgy and purification factory in China, with over 60 years of U mining history, and its neighboring U-contaminated soil was used as a sampling site. Soil samples were collected in accordance with the Soil Environmental Quality Standard (GB15618-1995). The stones, dead branches, and residual roots in the soils were removed before being placed in an artificial climate incubation chamber to carry out potting experiments. *V. zizanioides*, a metalloid-tolerant plant species capable of recruiting specific rhizosphere microorganisms to alleviate heavy metal stress and coupling nitrogen biotransformation with metal detoxification (Yu et al., 2025), was used as the test plant, with a soil content of 8.0 kg pot^{-1}. Under equal nitrogen conditions of 1.0 g pot^{-1}, we construct 8 treatments: (1) no fertilizer (CK), (2) 100% inorganic fertilizer (IF), (3) 100% sheep manure organic fertilizer (SOF), (4) 100% FOF, (5) 20% inorganic fertilizer substitution with FOF ($FOF_{0.2}$+$IF_{0.8}$), (6) 40% inorganic fertilizer substitution with FOF ($FOF_{0.4}$+$IF_{0.6}$), (7) 60% inorganic fertilizer substitution with FOF ($FOF_{0.6}$+$IF_{0.4}$), (8) 80% inorganic fertilizer substitution with FOF ($FOF_{0.8}$+$IF_{0.2}$). All experiments were carried out in four replicates, resulting in a total of 32 potted plants (Fig. S1). FOF was

the organic fertilizer made by drying and screening the mature products of food waste composting obtained from our previous research (Wu et al., 2022a). Inorganic fertilizer (IF) was acquired from Anhui Fumin Biological Organic Fertilizer Co., Ltd. Sheep manure organic fertilizer (SOF) was obtained from Anyang Zhongying Fertilizer Co., Ltd. *Vetiveria zizanioides* seedlings (approximately 10 cm tall) were purchased from the nursery of the Institute of Red Soil, Jiangxi, China. The *V. zizanioides* seedlings were first cultured in unpolluted soil, watered regularly. At the beginning of the formal experiment, similar growing *V. zizanioides* seedlings (about 15 cm) were selected and transplanted, with a soil content of approximately 20 g per plant. Both the IF and organic fertilizer were applied as a single basal dose prior to transplanting *V. zizanioides*. The basic properties of soils and various fertilizers are listed in Table S1.

2.2. Collection and pretreatment of soil and plant samples

The pot experiment was conducted from June 2024 for a duration of 60 days. Soil samples were collected at three stages: transplantation (day 1), vigorous growth (day 30), and maturity (day 60). At each sampling date, three of the four replicate pots per treatment were randomly selected and destructively harvested. Surface (0 ~ 10 cm) soil samples were collected using a multi-point sampling method. Approximately 100 g of soil was taken from each pot, and root litter and surface impurities were removed. Prior to testing, the soil samples were air-dried, ground, and passed through a 0.15 mm sieve. We determined soil properties across all sampling stages for each treatment, including soil organic matter (SOM), available nitrogen (AN), available phosphorus (AP), available potassium (AK), pH and redox potential (Eh), as well as total U content and U speciation.

After 2 months, plants from each group were randomly collected for the determination of root length and plant height. Additionally, the plant samples were divided into three parts: roots, stems and leaves. 10 g of tissue samples were taken from each part, soaked in EDTA-2Na for 20 min, rinsed with deionized water, and then dried in a 105°C oven for 30 min. Following additional grinding and crushing, the samples were ashed for 5 h at 600°C in a muffle furnace, cooled, and then utilized for U determination.

2.3. Determination of plant physicochemical parameters and U content

Soil pH and Eh were directly measured by means of a pH meter using a water:soil ratio of 2.5:1 (v/w) and platinum electrode, respectively (Halvorson et al., 2011). Potassium dichromate volumetric method, alkaline diffusion method, hydrochloric acid ammonium fluoride (HCL-NH_4F) method, and ammonium acetate (NH_4OAc) extraction flame photometer were used to measure the concentration of SOM, AN, AP, and AK, respectively (Hu et al., 2014; Zhao et al., 2023). The following steps were taken for the determination of U content in soil: 200 mg of air-dried soil sample was weighed into a polytetrafluoroethylene (PTFE) digestion tube, and 6 mL of HNO_3, 2 mL of HCl, and 2 mL of HF were then added to the tube to drive the acid (150°C for 7 min). Subsequently, the digestion tube was placed in a microwave digestion apparatus for digestion. Lastly, the digested supernatant was filtered through 0.22 μm microporous membrane and analyzed for U content using an inductively coupled plasma mass spectrometer (ICP-MS, Agilent 7700x, USA). The occurrence forms of U in soil were determined using the

Tessier method, which includes five fractions: exchangeable U, U bound to carbonates, U bound to Fe-Mn oxides, U bound to organic matter, and residual U. The detailed determination method was based on a previously reported procedure (Hu et al., 2024).

The BC0990 kit was implemented to measure the chlorophyll content of *V. zizanioides*. The total chlorophyll content is the sum of the absorbance values of the leaf sample at 645 nm and 663 nm, which represent the content of chlorophyll a and b, respectively. The activities of superoxide dismutase (SOD), peroxidase (POD) and catalase (CAT) in plants were detected using SOD kit (Nanjing Jiancheng), POD kit (Shanghai Yushao Biotechnology Co., Ltd.), and CAT kit (Shanghai Zeye Biotechnology Co., Ltd.), respectively. Following the above digestion procedures for soil sample, 0.2 g of ashed samples from different plant tissues were precisely weighed and digested. The supernatant was further filtered through a 0.22 μm microporous membrane and evaluated for U content utilizing ICP-MS (Agilent 7700x, USA). The following formula was used to calculate the translocation factor of *V. zizanioides*:

$$\text{Translocation factor} = \text{U content in aboveground part of plant} / \text{U content in plant roots} \quad (1)$$

2.4. Soil microbial DNA extraction, amplicon sequencing and data analysis

On days 1, 30, and 60, rhizosphere soil samples were gathered from the eight groups for the purpose of analyzing the microbial diversity and community structure. After removing large particulate matter and broken root fragments, five g of each sample with three replicates was taken and stored in a -80°C refrigerator, generating a total of 72 samples for DNA extraction. Following the manufacturer's instructions, genomic DNA was extracted employing the E.Z.N.A.® Soil DNA Kit (Omega Bio-tek, Norcross, GA, U.S.), and then the amount and quality of DNA were assessed by a NanoDrop 2000 Spectrophotometer (Bio-Rad Laboratories Inc., USA.). The bacterial 16S rRNA gene's V3-V4 region was amplified by PCR utilizing primer pairs of 341F 5'-CCTAYGGGRBGCASCAG-3' and 806R 5'-GGACTACNNGGGTATCTAAT-3' (Wu et al., 2022b). The AxyPrep DNA Gel Extraction Kit (Axygen Biosciences, Union City, CA, U.S.) was subsequently implemented to purify amplicons, which were extracted from 2% agarose gels. The purified PCR products were finally paired-end sequenced on an Illumina NovaSeq PE250 platform in Shanghai BIOZERON Co., Ltd adopting the standard protocols. The raw data of 16S rRNA gene amplicon was deposited into the NCBI SRA database with accession number of SRP547281.

The raw Illumina NovaSeq sequencing data of 16S rRNA gene was processed utilizing the QIIME software tool (version 1.8.0) (Qi et al., 2022). After filtering reads based on quality scores (< 20) and sequence lengths (< 400 bp), high-quality and chimera-free sequences were obtained from the NovaSeq platform via 16S rRNA gene sequencing. To find indel-mutations and substitutions, the passed sequences were dereplicated and run through the DADA2 algorithm (Edgar, R.C., 2010). Paired-end reads were trimmed and filtered allowing a maximum of two expected errors. Distinct Amplicon Sequence Variants (ASVs) were then inferred after merging paired reads and removing chimeras (Luo et al., 2022).

The ASVs feature table and feature sequence served as the foundation for the subsequent analysis of microbial community diversity and structural succession.

2.5. Metagenome assembly, binning, functional annotation

To further explore the functional gene response characteristics of the rhizosphere microbial community, metagenomic sequencing was performed on rhizosphere soil samples collected from the CK, IF, $FOF_{0.6}$+$IF_{0.4}$, and SOF groups at days 1 and 60. Three biological replicates were included for each treatment, resulting in a total of 24 samples, with each sequenced to a depth of 50 G. Raw metagenomic reads were quality-filtered using the Read_qc module implemented in metaWRAP (version 1.2.1). Clean reads were then *de novo* assembled into contigs using MEGAHIT (version 1.1.3) with a range of k-mer sizes from 21 to 141 (step = 12), and only contigs exceeding 500 bp were retained for downstream analyses (Uritskiy et al., 2018). Prodigal (v2.6.3) was employed to predict open reading frames (ORFs) from the assembled contigs. Predicted proteins were functionally annotated against the KEGG database (release 94.2) via DIAMOND BLASTx (e-value ≤ 10^{-5}) (Hu et al., 2024). Gene abundances were quantified as transcripts per million (TPM) using Salmon (v0.13.1).

Genome binning was performed using three independent binners, CONCOCT (version 0.4.1), MaxBin2 (version 2.2.4), and MetaBAT2 (version 2.12.1) based on GC content, scaffold coverage, and tetranucleotide frequencies). The resulting bins were consolidated and refined using the *bin_refinement* module of metaWRAP, followed by the *Reassemble_bins* module to generate high-quality metagenome-assembled genomes (MAGs) (Kang et al., 2019). The quality of the MAGs was evaluated using CheckM2, and only those with a completeness of > 90% and contamination of < 5% were retained for downstream analysis (Johnston et al., 2019). Salmon (version 0.13.1) was used to quantify the relative abundance of each MAG, reported as genome copies per million reads. KEGG functional annotation of individual MAGs was performed by aligning their Prodigal-predicted genes against the database using DIAMOND BLASTx (e-value ≤ 10^{-5}). To validate the completeness of KEGG-Decoder-inferred pathways, MAGs were functionally annotated against METABOLIC (version 4.0) for the principal biogeochemical cycles (El-Gebali et al., 2019). Taxonomic assignment of all MAGs was performed using the *classify_wf* module of GTDB-Tk (version 2.1.0). Structural equation modeling (SEM) was applied to reveal the links between key microbial communities, biogeochemical cycling, and U fate. The data of metagenome sequencing was deposited into the NCBI SRA database with accession number of PRJNA1183910.

2.6. Statistical analysis and data visualization

Mothur v.1.21.1 was employed to disclose the diversity indices, which included the Chao1 and Shannon diversity indices (Schloss et al., 2009). Principal coordinate analysis (PCoA) based on Bray-Curtis distance matrice was performed using the vegan package in R (https://r-forge.r-project.org/) to compare the compositional variation in microbial communities (Yu et al., 2025). The microbial co-occurrence networks at the phylum level were constructed based on Spearman's rank correlation coefficients using the linkET package in R. To ensure robust correlations, only pairs with a correlation coefficient $|r| > 0.6$ and a significance level of $P < 0.05$ were retained for network visualization. The enrichment ratio of

bacterial taxa was calculated and visualized using R software with the ggplot2 package (version 3.5.0), and significant differences were identified using non-parametric Kruskal-Wallis tests. Excel 2016 and Origin 2021 were utilized to handle all experimental data, and the results were shown as mean ± standard error of the triplicate. The statistically significant level was considered at $P < 0.05$.

3. Results and discussion

3.1. Effects of FOF on physicochemical properties of U-contaminated soils

Soil pH and Eh are critical regulators of U speciation and bioavailability (Pentyala et al., 2020). The pH in CK group remained consistently between 7.88 and 7.96 (Fig. 1a), indicating a slightly alkaline environment. The Eh value decreased from − 45.97 mV to -61.70 mV (Fig. 1b), gradually shifting toward reducing conditions. Reductive condition favors the formation of stable, insoluble U(IV) precipitates, thereby limiting U bioavailability for plant uptake (Huang et al., 2024). In IF group, pH dropped markedly to 6.1 on the 60th day due to the release of hydrogen ions from IF dissolution (Qian et al., 2023), while Eh (-38.27 mV) remained slightly higher than the control. In FOF, SOF, and the combined-application groups, pH ranged from 7.12 to 7.57, significantly ($P < 0.05$) lower than that in the CK group. Among these, the $FOF_{0.6}$+$IF_{0.4}$ group exhibited the lowest pH (7.13) on day 60, presumably due to the neutralizing effect of humic acid contained in the organic fertilizer (Xiao et al., 2025). Regarding Eh, all organic fertilizer groups showed substantially ($P < 0.05$) higher values than both CK and IF groups. The $FOF_{0.6}$+$IF_{0.4}$ treatment group had the highest Eh value (-20.37 mV) at day 60, representing a 70.0% increase compared with the control. This change was primarily attributed to the improvement of soil structure and aeration by organic fertilizer, which subsequently elevated soil Eh (Zhu et al., 2021). Collectively, FOF (particularly $FOF_{0.6}$+$IF_{0.4}$) effectively prevented the rhizosphere from entering a highly reductive state. This elevated Eh and moderately decreased pH collectively maintained U in its more mobile U(VI) form, establishing a favorable chemical prerequisite for subsequent root uptake.

SOM can not only reduce the bioavailability and toxicity of heavy metals through complexation and adsorption, but also support soil microbial activity and plant metabolism by releasing long-lasting carbon sources, thereby enhancing the remediation of U-contaminated soils (Dangelmayr et al., 2019; Edayilam et al., 2020). The SOM content in the CK group remained stable at 50.56 ~ 53.10 g kg^{-1}, with only marginal increases in the IF group, indicating that IF did not significantly promote SOM accumulation (Fig. 1c). In contrast, the FOF treatment exhibited markedly ($P < 0.05$) higher SOM contents than other treatments at day 60, reaching 125.10 g kg^{-1}, corresponding to increases of 135.62% relative to the control. This can be attributed to the inherently high organic matter content (76.61%) in FOF, coupled with its slow decomposition rate, which sustains soil organic matter levels over long term (Wang et al., 2025). The combined FOF + IF treatments showed a progressive increase in SOM content with rising FOF proportion. Cumberland et al., reported that dissolved organic matter (DOM) could migrate to U surface and act as a barrier film, preventing its adsorption by soil solids and thereby

enhancing U mobility and bioavailability (Bone et al.,2020). Given that organic fertilizers release substantial amounts of DOM during decomposition (Fan et al.,2025), the elevated SOM in FOF-containing treatments likely includes a higher proportion of DOM, thus benefiting U uptake by *V. zizanioides*.

Available nutrients (e.g., AN, AP, and AK) are fundamental for plant growth and directly regulate the efficiency of U accumulation (Tan et al., 2025). In the CK group, AN content remained at 238 ~ 247 mg kg^{-1}, indicating a stable but relatively low level of nutrient supply (Fig. 1d). The IF group exhibited an initial AN peak of 512.5 mg kg^{-1}, representing a 107.49% increase over the control. However, this level declined to 473.25 mg kg^{-1} on day 60. This reduction is ascribed to the susceptibility of inorganic nitrogen to plant uptake and leaching loss, which precludes a sustained release (Fang et al., 2021). The AN content in FOF, SOF, and combined application groups were significantly ($P < 0.05$) higher than that of the control. Among these, the $FOF_{0.6}$+$IF_{0.4}$ treatment exhibited the highest AN, AP, and AK contents (630.5, 290.48, and 431.14 mg kg^{-1}, respectively) at day 60, corresponding to increases of 157.35%, 117.5%, and 118.81% relative to the control (Fig. 1e and 1f). These findings suggest that FOF supplies abundant NPK nutrients intrinsically and facilitates the activation of refractory nutrients by ameliorating soil structure and the microbial community composition (Du et al., 2022). The combined application of FOF and IF generates synergistic supply of readily available nutrients (from IF) and slow-release nutrients (from FOF), meeting rapid nutrient demands during early growth stages while sustaining nutrient availability in later stages (Yang et al., 2025). At day 60, the SOF group exhibited AN, AP, and AK contents of 576.25, 274.73, and 460.44 mg kg^{-1}, respectively, which were consistently lower than those in the FOF, and high-ratio combined application groups. This phenomenon may be attributed to the fact that the nutritional supply capacity of FOF is superior to SOF, which is consistent with its higher organic matter and available nutrient content. Therefore, by promoting plant growth and biomass accumulation, the elevated available nutrients in FOF-treated soils (especially $FOF_{0.6}$+$IF_{0.4}$) indirectly increased U removal from contaminated soils.

3.2. FOF promotes the growth of *V. zizanioides* and enhances U uptake and translocation

Root length and plant height are important indicators reflecting plant growth and stress tolerance. Under U stress, the growth of *V. zizanioides* was markedly inhibited in the CK group, with root length and plant height reaching only 12.50 cm and 79.75 cm, respectively (Fig. 2a and 2b). The IF group showed limited growth promotion (root length: 23.50 cm; plant height: 89.63 cm), which was attributed to its inability to improve soil structure and susceptibility to nutrient loss (Zhao et al.,2024). In contrast, organic fertilizer treatments substantially enhanced the growth of *V. zizanioides*: in the SOF and FOF groups, root length increased by 183.2% and 216.24%, respectively, while plant height increased by 52.58% and 59.35%, respectively. The combined application groups achieved even greater efficacy, with the $FOF_{0.6}$+$IF_{0.4}$ treatment exhibiting optimal performance (root length: 52.13 cm; plant height: 146.48 cm; increases of 317.04% and 83.63% over the control, respectively), followed by $FOF_{0.8}$+$IF_{0.2}$. This pronounced root

proliferation is critically important. It not only expands the soil volume explored for U uptake but also reflects the alleviation of U-induced root toxicity in the FOF-amended rhizosphere (Gupta et al., 2020). This synergistic effect arises from the complementary roles of IF and FOF. IF supplies readily available nutrients for early-stage plant demand, while FOF improve soil structure, regulate pH, and provide sustained nutrient release (Yang et al., 2025).

The improvement in plant physiological status further corroborates the establishment of a low-stress microenvironment. As shown in Fig. 2c, the CK group exhibited the lowest chlorophyll content (0.97 mg g^{-1}). The results confirm that U toxicity suppresses chlorophyll synthesis, which is potentially mediated by oxidative stress. Oxidative stress impairs chloroplast structure and inhibits biosynthetic enzymes such as Mg^{2+} chelatase and δ-aminolevulinic acid dehydratase (ALAD) (Kolhi et al., 2026). The IF group showed only a modest increase (1.18 mg g^{-1}). In contrast, the treatments involved only organic fertilizers or combined with IF, led to substantially higher chlorophyll contents, with the $FOF_{0.6}$+$IF_{0.4}$ treatment exhibiting the highest value (1.70 mg g^{-1}), followed by $FOF_{0.8}$+$IF_{0.2}$ (1.64 mg g^{-1}), FOF (1.54 mg g^{-1}), and SOF (1.43 mg g^{-1}). The advantages of combined treatments can be attributed to two factors. First, the improvement in soil physicochemical properties alleviated the inhibition of chlorophyll synthesis enzymes by U (Hu et al., 2023). Second, the slow-release nitrogen from organic fertilizers promoted chlorophyll biosynthesis and maintained its stability (Kudpeng et al., 2025). Elevated chlorophyll content in $FOF_{0.6}$+$IF_{0.4}$ treatment implies enhanced photosynthetic capacity and biomass accumulation, thereby providing the material foundation for U uptake and enrichment (Xiong et al., 2025).

Upon exposure to U stress, plants typically activate their antioxidant enzyme systems to scavenge overproduced reactive oxygen species (ROS) and alleviate oxidative damage (Hu et al., 2019). In this study, the CK group displayed the lowest activities of SOD, POD, and CAT (113.67, 19.87, and 56.67 U g^{-1}, respectively) (Fig. 2d-2f), indicating limited activation of the endogenous antioxidant system under U stress. In the IF group, the activities of SOD, POD, and CAT showed only a slight increase (114.90, 328.50, and 59.83 U g^{-1}, respectively), suggesting that IF alone was insufficient to trigger a strong antioxidant response in plants (Liu et al., 2025). Organic fertilizer treatment significantly boosted antioxidant enzyme activities, with the FOF group (118.80, 382.53, 66.93 U g^{-1} of SOD, POD, and CAT) performing slightly better than SOF (116.37, 367.40, 63.77 U g^{-1} of SOD, POD, and CAT). The combined treatments had the highest antioxidant capacity. The activity of SOD, POD, and CAT in the $FOF_{0.6}$+$IF_{0.4}$ treatment was 121.13, 402.17, and 70.50 U g^{-1}, respectively, representing increases of 6.56%, 25.73%, and 24.40% over the control, followed by $FOF_{0.8}$+$IF_{0.2}$ (119.40, 393.53, 66.03 U g^{-1}). While previous studies often attribute such enhancements solely to nutrient supply (Liu et al., 2024), our results suggest a more complex mechanism. The enriched antioxidant capacity and stable chlorophyll synthesis indicate that FOF effectively mitigates U-induced oxidative damage, providing the physiological foundation for biomass accumulation and subsequent metal enrichment.

Phytoremediation efficiency is ultimately determined by the reduction of residual U in soil and its accumulation in plant tissues (Liao et al., 2022). Results showed a strong positive correlation between FOF application rate and U removal efficiency (Fig. S2). The $FOF_{0.6}$+$IF_{0.4}$ treatment achieved the lowest residual soil U content (62.88 mg kg^{-1}) with a removal rate of 64.67%. In this group, the U concentrations in roots, stems, and leaves were 42.13 mg kg^{-1} (Fig. 2g), 40.35 mg kg^{-1} (Fig. 2h), and 28.20 mg kg^{-1} (Fig. 2i), respectively, representing a 218.6% increase in total U accumulation compared with the control. Although all treatments exhibited the general distribution pattern where the root biomass was greater than the shoot biomass, the combined application significantly ($P < 0.05$) promoted U translocation from roots to aboveground tissues. Furthermore, the translocation factor (TF) in the $FOF_{0.6}$+$IF_{0.4}$ treatment reached 1.627, far exceeding those in the CK and IF groups (below 0.84) (Fig. S3). This indicates that FOF not only promotes root uptake but also effectively facilitates the root-to-shoot translocation of U, which is a critical bottleneck for efficient phytoextraction (Chen et al., 2023). Collectively, by improving soil physicochemical properties and establishing a low-stress rhizosphere niche, the $FOF_{0.6}$+$IF_{0.4}$ treatment maximized both plant biomass and U accumulation, identifying it as the optimal strategy for the phytoremediation of U-contaminated soils.

3.3. FOF-driven temporal succession and targeted enrichment of keystone functional taxa

The diversity of microbial community is an important indicator reflecting the response of soil ecosystems to fertilization treatments (Hartmann et al., 2023). PCoA clearly showed that fertilization treatments significantly reshaped the rhizosphere microbial community structure (PERMANOVA, R^2 = 0.46, $P < 0.001$), explaining 22% of the total variation (Fig. 3a). The FOF treatment formed a cluster that was spatially separated from both the IF and SOF groups, and all fertilized treatments were significantly differentiated from the control. Furthermore, an independent PCoA across the substitution ratio gradient ($FOF_{0.2}$ to $FOF_{0.8}$) revealed a continuous trajectory in community composition (PERMANOVA, R^2 = 0.45, $P < 0.001$) (Fig. 3b). This continuous gradient indicates that different organic-inorganic ratios selectively drive divergent community assembly processes by providing distinct niche preferences.

Fertilization treatments exerted differential effects on the α-diversity of the rhizosphere bacterial community. As shown in Fig. 3c, the Shannon index exhibited relative stability across different fertilization modes and substitution ratios. No significant differences were observed among the four main treatments (CK, FOF, IF, and SOF) ($P > 0.05$), indicating that fertilization did not drastically disrupt community evenness. Within the combined application groups, the $FOF_{0.6}$+$IF_{0.4}$ group maintained a high Shannon index, particularly on day 60, suggesting a higher degree of structural evenness and stability under this specific ratio. The variation trend of microbial richness (Chao1 index) was generally consistent with that of the Shannon index (Fig. 3d). Although no statistically significant differences were found among the four main treatments (CK vs. FOF/IF/SOF), microbial richness within the combined application groups showed an overall increasing trend with the rise in organic fertilizer substitution ratios. Notably, the Chao1 index of the $FOF_{0.6}$+$IF_{0.4}$ group remained at a high level. While slightly lower

than that of the $FOF_{0.8}$+$IF_{0.2}$ group, the $FOF_{0.6}$+$IF_{0.4}$ group achieved an optimal synergy between species richness and community evenness when considering both indices. This finding aligns with the report by Hei et al. (2023), in which the continuous input of exogenous microorganisms and nutrients from organic fertilizer application drove the proliferation of specific bacterial taxa, subsequently influencing the filtration and assembly of the rhizosphere microbial community. Consequently, the 60% organic substitution ratio effectively promotes microbial colonization through exogenous organic input while avoiding potential ecological imbalances associated with excessive application, thereby serving as the optimal strategy for maintaining rhizosphere micro-ecological health and stability.

The temporal dynamics of the rhizosphere microbiome not only responds to abiotic stresses (e.g., heavy metal toxicity, nutrient imbalance), but also undergoes successional reorganization along with plant growth, thereby regulating nutrient acquisition and stress resistance (Trivedi et al., 2020). Figure 3e showed the changes in microbial community structure at genus level in the rhizosphere of *V. zizanioides*. The top seven genera were *Luteitalea*, *Sphingomonas*, *Vicinamibacter*, *OLB13*, *Pseudomonas*, *RB41*, and *Gemmatimonas*. On day 1, the relative abundance of *Pseudomonas* increased markedly in the FOF, SOF, and combined application treatments. This rapid response indicates that the labile carbon and nutrients introduced by FOF and SOF immediately activated this genus, which is known for its dual ecological functions, including U detoxification and plant growth promotion such as phosphate solubilization and IAA secretion (Kasko et al., 2023; Meliani et al., 2017). This early-stage enrichment serves as a rapid biological strategy to passivate U toxicity and provide essential nutrient support for plant establishment.

As the plant entered the vigorous growth stage (day 30), the $FOF_{0.6}$+$IF_{0.4}$ treatment exhibited a unique successional trajectory, with *Pseudomonas* emerging as the absolutely dominant genus (14.32%), far exceeding the control (0.26%) and other treatments. This massive and specific proliferation suggests that FOF provides a highly favorable substrate niche for *Pseudomonas*, driving it to become the primary engine for U mobilization and nutrient cycling during this critical growth phase. By day 60, the community structure diverged further. The CK group was dominated by stress-adapted indigenous genera such as *Vibrinimonas* (6.79%), *Luteitalea* (6.73%) and *OLB13* (3.87%), reflecting a passive reorganization under oligotrophic and U-stressed conditions (Abdelkrim et al., 2020). In contrast, the groups treated with organic fertilizer, particularly in the FOF groups, exhibited notably different succession patterns. Compared to the CK group, the SOF treatment exhibited higher relative abundances of *Luteitalea* and *Sphingomonas*, with increases of 44.68% and 23.66%, respectively. *Sphingomonas* contributes to U detoxification and immobilization through U(VI) reduction, organic acid complexation, and extracellular fixation (Chen et al., 2025). This explains the lower U phytoextraction efficiency in SOF, as its driven microbiome primarily drives U toward sequestration pathways rather than mobilization pathways.

Conversely, the $FOF_{0.6}$+$IF_{0.4}$ treatment maintained a high relative abundance of a distinct functional consortium composed of *Pseudomonas*, *Sphingomonas*, and *Gemmatimonas* (totaling 4.96%, higher than the control). The co-enrichment of these three taxa at the mature stage is not coincidental, but rather reflects a sophisticated functional partitioning. *Gemmatimonas* dominates the decomposition of SOM

and phosphorus activation, providing critical available carbon sources and effective phosphorus for microbial communities under environmental stress (Hu et al., 2021). Previous studies have demonstrated that organic substitution can activate beneficial functional microbes. This is achieved by providing organic substrates, facilitating nutrient cycling, and improving soil structure and fertility, which consequently enhances soil quality and crop yield (Cao et al., 2023; Liu et al., 2022). Consequently, the $FOF_{0.6}$+$IF_{0.4}$ treatment disrupted the natural succession of the indigenous community and assembled a functional microbiome specialized for U detoxification, P activation, and plant growth promotion. This temporally structured community assembly provides a robust microbiological foundation for the synergistic coupling of detoxification and extraction observed in this study.

3.4. Response characteristics of rhizosphere microbial functional genes to FOF addition

Metagenomic analyses were performed to evaluate the effects of fertilization treatments on the rhizosphere microbial functional genes involved in heavy metal transformation, phosphorus (P), sulfur (S), and nitrogen (N) cycling. The biogeochemical fate of U is highly dependent on microbial metal transformation pathways (Yuan et al., 2022). As shown in Fig. 4a and Fig. S5, the relative abundance of U reduction genes (*MtrB*, *MacA*, *ccoN* and *qcrC*) in the CK group was significantly ($P < 0.05$) higher than that in the FOF-treated soils. This indicates that under oligotrophic conditions, indigenous microorganisms utilize U reduction as a critical strategy for detoxification and energy acquisition, reflecting a survival-prioritized adaptive response to resource limitation (Zhang et al., 2025). Conversely, although the $FOF_{0.6}$+$IF_{0.4}$ treatment achieved superior U removal, its relative abundance of U reduction genes was notably suppressed. This strongly suggests that the enhanced U phytoextraction in FOF-treated soils is not primarily driven by microbially mediated reductive precipitation, which would otherwise immobilize U. Instead, FOF significantly ($P < 0.05$) increased the relative abundance of heavy metal resistance and efflux genes (*azr*). This functional shift implies that FOF mitigates U biotoxicity by enhancing the active defense and electron transfer capabilities of the microbial community, thereby establishing a low-stress rhizosphere niche (Li et al., 2025). In stark contrast, the SOF treatment exhibited the highest relative abundance of U reduction genes. This result demonstrates that SOF predominantly drives U immobilization by providing sufficient carbon sources that strongly stimulate the reductive metabolic potential of the microbial community.

The functional potential for P acquisition was also significantly reprogrammed (Fig. 4b). In the CK group, the higher relative abundance of P solubilization (e.g., *gcd*, *ppa*, *ppk*), transportation (e.g., *pst* family, *ugpA* and *ugpB*), and regulation (*gcd*, *pst* family and *phoB*) was observed, indicating severe P starvation that stimulated fierce microbial competition for limited P supplies (Yu et al., 2025). In contrast, the $FOF_{0.6}$+$IF_{0.4}$ treatment induced a distinct shift towards organic P mineralization (e.g., *appA* and *phn* family) (Fig. S5). This indicates that the organic components in FOF not only directly supply nutrients but also stimulate the microbial community to unlock soil legacy P pools through enhanced solubilization and mineralization processes (Hu et al., 2024). The resulting massive release of orthophosphate serves a dual purpose: it provides essential nutrients for plant growth, and it acts as a frontline detoxification

mechanism by precipitating uranyl ions in localized root zones, alleviating U phytotoxicity (Tan et al., 2024).

S cycling redox processes can directly influence U valence and bioavailability through their metabolites such as sulfides and thiosulfates (Zhang et al., 2023). Variations in the abundance of genes associated with assimilatory S reduction, dissimilatory S reduction and oxidation, and the S oxidation system (SOX) were analyzed (Fig. 4c). In the CK group, the high relative abundance of dissimilatory S reduction genes (*aprA/B*, *dsrA/C*, etc.) was consistent with its reducing microenvironment (Eh = -61.70 mV), suggesting a high potential for the generation of toxic sulfides. In the SOF group, S oxidation genes (*cys* family, *sox* family, etc.) were significantly ($P < 0.05$) increased. Conversely, the $FOF_{0.6}$+$IF_{0.4}$ treatment suppressed dissimilatory S reduction and shifted towards assimilatory pathways. This functional shift is ecologically significant, as it redirects microbial S metabolism from toxicity-generating processes toward biomass-assimilating pathways (Gorvel et al., 2025). Consequently, it avoids H_2S phytotoxicity and maintains rhizosphere redox stability, thereby favoring root proliferation.

Regarding N cycling genes, the $FOF_{0.6}$+$IF_{0.4}$ and SOF treatments significantly elevated the abundance of the N fixation gene *nifK*, while suppressing the anammox gene *hzsA* (which was highly enriched in the CK group). Yang et al. also reported that organic fertilizer increased the abundance of *nifK* by 1.5-3.0 fold (Yang et al., 2025). This result indicated that FOF and SOF may enhance N retention by promoting N-fixation potential and suppressing N loss (Farzadfar et al., 2021). More importantly, the intermediate products of N transformation can act as alternative electron acceptors. This thermodynamically outcompetes U(VI) for microbial reduction, thereby maintaining a higher proportion of mobile U(VI) in the rhizosphere solution for continuous plant uptake (Wang et al., 2024). Consequently, these functional gene profiles demonstrate that FOF orchestrates a coordinated metabolic strategy: suppressing U reduction, enhancing metal efflux, activating P mineralization, and redirecting S/N cycling to sustain a bioavailable U(VI) pool.

3.5. Synergistic regulation of uranium fate by phosphorus-mediated detoxification and microbial mobilization

To quantitatively decipher how the keystone genera (*Gemmatimonas*, *Pseudomonas*, and *Sphingomonas*) regulate U fate through biogeochemical cycling, a structural equation model (SEM) was constructed (Fig. 5). The SEM demonstrated an excellent fit to the data (Goodness of fit = 0.745), explaining 44.3%, 88.0%, 93.2%, and 20.5% of the variance in N cycling, S cycling, P function, and metal metabolism, respectively. Notably, the model accounted for 98.6% and 96.6% of the variance in plant U content and soil U content, respectively, indicating a robust representation of U dynamics.

As the upstream driver of rhizosphere biogeochemical processes, the keystone microbial community exhibited distinct regulatory effects on nutrient cycling modules. A significant negative direct effect was observed on N cycling (path coefficient = -0.675, $P < 0.05$), implying that the FOF-amended microbiome actively suppresses N-loss pathways and promotes the accumulation of intermediate products (e.g.,

NO_2^-) (Zhang et al., 2022). Conversely, non-significant positive or negative associations were detected for metal metabolism (0.453), S cycling (0.010), and P function (-0.266). Among the four biogeochemical modules, P function was the strongest and most significant predictor of soil U content (path coefficient = 1.318, $P < 0.01$). This robust positive effect indicates that enhanced P solubilization and mineralization processes substantially increase U sequestration in the rhizosphere. To elucidate the specific microbial drivers underlying this biogeochemical process, we reconstructed high-quality bacterial MAGs (completeness > 90%, and contamination < 5%) from the rhizosphere samples (Fig. S6). The massive release of orthophosphate (PO_4^{3-}) driven by P mineralization genes (e.g., *phoD* and *phnG* in bin.18) (Fig. S6a) exerts a dual action: it directly supplies bioavailable P for *V. zizanioides* growth, and it reacts with U to form highly insoluble U-phosphate precipitates (Mishra et al., 2026). This P-driven in-situ precipitation acts as a frontline detoxification mechanism, drastically reducing the labile, phytotoxic uranyl ions in the pore water and creating a low-stress niche that supports root proliferation (Misson et al., 2009). Similar coupling between organophosphorus mineralization and uranate immobilization has been recently documented in actinobacterial taxa recovered from uranium tailings (Hu et al., 2024).

Conversely, metal metabolism (-0.287), S cycling (-0.455) and N cycling (-0.716) were negatively associated with soil U content, collectively contributing to U mobilization in the rhizosphere. Consistent with the enhanced expression of Fe(III) reduction, electron transport, and heavy metal resistance and efflux genes (*efeU*, *copA*, *czcA*, and *azr*) (Fig. S6a), microbial metal metabolism may indirectly couple dissimilatory Fe(III) reduction with the reductive dissolution of U-bearing iron oxides, thereby releasing U from solid phases (Li et al., 2025). Crucially, the strong negative path of N cycling (-0.716) directly validates our previous hypothesis derived from the functional gene profiles. It indicates that the active N transformation process (e.g., NO_2^- accumulation) thermodynamically suppresses the microbial reduction of U(VI) by outcompeting it for electrons, thereby maintaining a higher proportion of mobile U(VI) in the rhizosphere solution (Hu et al., 2024; Zhang et al., 2022). Taken together, these four functional pathways explained 96.6% of the variance in soil U content, underscoring that U fate is balanced between P-driven dual roles of growth promotion and localized detoxification, and the mobilization driven by metal and N cycling.

Regarding plant uptake, the SEM revealed a significant direct negative path from soil U content to plant U content (path coefficient = -1.033, $P < 0.05$), reflecting the depletion of the soil U pool driven by intensive root uptake. Importantly, the keystone microbial community exhibited a highly significant direct negative effect on soil U content (path coefficient = -0.688, $P < 0.01$). *Sphingomonas* has been reported to mediate U detoxification via reduction and complexation, likely providing localized protection to the root apex (Chen et al., 2025). In contrast, *Pseudomonas* and *Gemmatimonas* may act as primary mobilizers, facilitating U release from solid phases into the rhizosphere solution via organic acid excretion and Fe(III) reduction (Bhatti et al., 2026). Collectively, this functional partitioning reshapes the biogeochemical fate of U, transforming the rhizosphere into a favorable environment for continuous root uptake and phytoextraction.

4. Conclusions

This study demonstrated that FOF is a superior amendment for enhancing the phytoremediation of U by *V. zizanioides* in contaminated soils (Fig. 6). Unlike traditional organic amendments like SOF that drive U immobilization, FOF orchestrates a sophisticated functional partitioning within the rhizosphere microbiome. By enriching key taxa (*Pseudomonas*, *Sphingomonas*, and *Gemmatimonas*), FOF establishes a synergistic coupling between phosphorus-mediated detoxification and microbial mobilization. Specifically, localized P mineralization precipitates U to alleviate phytotoxicity and support root growth, while microbial metal metabolism and N cycling actively mobilize U from soil solids into the rhizosphere solution. This dual functionality distinguishes FOF from IF and SOF. This study provides a novel mechanistic framework linking organic amendment-driven microbial nutrient cycling to pollutant fate in the rhizosphere, thereby highlighting the valorization of food waste for enhancing soil fertility and bioremediation.

Declarations

Authorship contribution

Xiaoyan Wu: Methodology, Conceptualization, Formal analysis, Data curation, Funding acquisition, Writing - original draft. Jian Liu: Methodology, Writing - original draft. Yingxuan Ouyang: Data curation, Writing - editing. Zhijun Zhang: Writing - review & editing, Supervision, Conceptualization. Guicheng He: Writing - review & editing, Investigation, Conceptualization. Lingling Wu: Writing – review & editing. Dandan Zhang: Writing – review & editing. Pubo Chen: Writing – review & editing. Qiaohong Chen: Writing – review. Huang Yu: Methodology, Writing – review & editing.

Acknowledgments

This work was supported by the National Natural Science Foundation of China (52404184), Deep Earth Probe and Mineral Resources Exploration-National Science and Technology Major Project (2025ZD1010700, 2025ZD1010708), Hunan Provincial Natural Science Foundation Youth Project (Category B) 527 (2026JJ40032) and Hunan Provincial Department of Education Outstanding Youth Project (No. 24B0397, No. 23B0422).

Conflict of interest

The authors declare that the research was conducted in the absence of any commercial or financial relationships that could be construed as a potential conflict of interest.

References

1. Abdelkrim S, Jebara SH, Saadani O, Abid G, Taamalli W, Zemni H et al (2020) In situ effects of lathyrus sativus- PGPR to remediate and restore quality and fertility of pb and cd polluted soils.

Ecotox Environ Safe 192:110260. https://10.1016/j.ecoenv.2020.110260

2. Abreu MM, Lopes J, Santos ES (2014) Ecotoxicity evaluation of an amended soil contaminated with uranium and radium using sensitive plants. J Geochem Explor 142:112–121. https://doi.org/10.1016/j.gexplo.2014.01.029
3. Akash S, Sivaprakash B, Raja VCV, Rajamohan N, Muthusamy G (2022) Remediation techniques for uranium removal from polluted environment -Review on methods, mechanism and toxicology. Environ Pollut 302:119068. https://doi.org/10.1016/j.envpol.2022.119068
4. Bhatti TM, Tuovinen OH (2026) Heterotrophic bacterial bioleaching and sequestration of uranium from mineral resources: a review. Front Microbiol 17:1803404. https://doi.org/10.3389/fmicb.2026.1803404
5. Bone SE, Cliff J, Weaver K, Takacs CJ, Roycroft S, Fendorf S et al (2020) Complexation by organic matter controls uranium mobility in anoxic sediments. Environ Sci Technol 54(3):1493–1502. https://doi.org/10.1021/acs.est.9b04741
6. Cao M, Duan Y, Li M, Cai G, Kan W, Li J et al (2023) Manure substitution improves maize yield by promoting soil fertility and mediating the microbial community in lime concretion black soil. J Integr Agric 223:698–710. https://doi.org/10.1016/j.jia.2023.05.040
7. Chandwadkar P, Acharya C (2023) Inorganic polyphosphate accumulation protects a marine, filamentous cyanobacterium, *Anabaena torulosa* against uranium toxicity. J Environ Radioact 263:107185. https://doi.org/10.1016/j.jenvrad.2023.107185
8. Chen HY, Sheng YZ, Wang SD, Chen Y, Qiao ZY, Guo HM et al (2025) Uranium contamination mediating soil and ore microbial community assembly at four mining sites, South China. Front Microbiol 16:1553072. https://doi.org/10.3389/fmicb.2025.1553072
9. Chen T, Yu KF, Dong CX, Yuan X, Gong X, Lian J et al (2022) Advanced photocatalysts for uranium extraction: elaborate design and future perspectives. Coord Chem Rev 467:214615. https://doi.org/10.1016/j.ccr.2022.214615
10. Chen X, Xia H, Lv J, Liu Y, Li Y, Xu L et al (2023) Magnetic hydrothermal biochar for efficient enrichment of uranium (VI) by embedding Fe_3O_4nanoparticles on bamboo materials from one-can strategy. Colloids Surf A. 658:130748. https://doi.org/10.1016/j.colsu rfa. 2022. 130748
11. Chi GY, Fang YT, Zhu B, Guo N, Chen X (2023) Intercropping with *Brassica juncea* L. enhances maize yield and promotes phytoremediation of cadmium-contaminated soil by changing rhizosphere properties. J Hazard Mater 461:132727. https://doi.org/10.1016/j.jhazmat.2023.132727
12. Cui QL, Zhang ZQ, Bei JZ, Cui YX, Chen L, Chen HS et al (2023) A critical review of uranium in the soil-plant system: distribution, bioavailability, toxicity, and bioremediation strategies. Crit Rev Env Sci Tec 53(3):340–365. https://doi.org/10.1080/10643389.2022.2054246
13. Dangelmayr MA, Figueroa LA, Williams KH, Long PE (2019) Characterizing organic carbon dynamics during biostimulation of a uranium contaminated field site. Biogeochemistry 143(1):117–132. https://doi.org/10.1007/s10533-019-00553-w

14. Du TY, He HY, Zhang Q, Lu L, Mao WJ, Zhai MZ (2022) Positive effects of organic fertilizers and biofertilizers on soil microbial community composition and walnut yield. Appl Soil Ecol 175:104457. https://doi.org/10.1016/j.apsoil.2022.104457
15. Edayilam N, Ferguson B, Montgomery D, Al Mamun A, Martinez N, Powell BA et al (2020) Dissolution and vertical transport of uranium from stable mineral forms by plants as influenced by the cooccurrence of uranium with phosphorus. Environ Sci Technol 54(11):6602–6609. https://doi.org/10.1021/acs.est.9b06559
16. Edgar RC (2010) Search and clustering orders of magnitude faster than BLAST. Bioinformatics 26(19):2460. https://doi.org/10.1093/bioinformatics/btq461
17. El-Gebali S, Mistry J, Bateman A, Eddy SR, Luciani A, Potter SC et al (2019) The Pfam protein families database in 2019. Nucleic Acids Res 47(D1):D427–D432. https://doi.org/10.1093/nar/gky995
18. Fang H, Liu KL, Li DM, Peng XH, Zhang WJ, Zhou H (2021) Long-term effects of inorganic fertilizers and organic manures on the structure of a paddy soil. Soil Tillage Res 213:105137. https://doi.org/10.1016/j.still.2021.105137
19. Fang Z, Yu HL, Li CH, Wang B, Jiao F, Huang JY (2023) Long-term phosphorus addition alters plant community composition but not ecosystem stability of a nitrogen-enriched desert steppe. Sci Total Environ 879:163033. https://doi.org/10.1016/j.scitotenv.2023.163033
20. Fan JL, Song R, Luo H, Wu HJ, Wu DM, Wang J et al (2025) DOM from eco-friendly fertilizers increases soil potential pathogen risk and shapes specific microbial populations under sprinkler and drip irrigation. Appl Soil Ecol 216:106546. https://doi.org/10.1016/j.apsoil.2025.106546
21. Farzadfar S, Knight JD, Congreves KA (2021) Soil organic nitrogen: an overlooked but potentially significant contribution to crop nutrition. PLANT SOIL 462:7–23. https://doi.org/10.1007/s11104-021-04860-w
22. Gorvel S, Walter B, Taylor JD, Unsworth RKF (2025) Functional roles of the seagrass (*Zostera marina*) holobiont change with plant development. Plants 14(11):1584. https://doi.org/10.3390/plants14111584
23. Gupta DK, Vukovic A, Semenishchev VS, Inouhe M, Walther C (2020) Uranium accumulation and its phytotoxicity symptoms in *Pisum sativum* L. Environ Sci Pollut Res 27(3):3513–3522. https://doi.org/10.1007/s11356-019-07068-9
24. Halvorson JJ, Gonzalez JM, Hagerman AE (2011) Repeated applications of tannins and related phenolic compounds are retained by soil and affect cation exchange capacity. Soil Biol Biochem 43(6):1139–1147. https://doi.org/10.1016/j.soilbio.2011.01.023
25. Haneklaus NH, Mwalongo DA, Lisuma JB, Amasi AI, Mwimanzi J, Bituh T et al (2024) Rare earth elements and uranium in Minjingu phosphate fertilizer products: Plant food for thought. Resour Conserv Recy 207:107694. https://doi.org/10.1016/j.resconrec.2024.107694
26. Hartmann M, Six J (2023) Soil structure and microbiome functions in agroecosystems. Nat Rev Earth Environ 4:4–18. https://doi.org/10.1038/s43017-022-00366-w

27. Hei Z, Peng Y, Hao S, Li Y, Yang X, Zhu T et al (2023) Full substitution of chemical fertilizer by organic manure decreases soil N_2O emissions driven by ammonia oxidizers and gross nitrogen transformations. Glob Change Biol 29:7117–7130. https://doi.org/10.1111/gcb.16957
28. Huang F, Dong F, Chen L, Zeng Y, Zhou L, Sun S et al (2024) Biochar-mediated remediation of uranium-contaminated soils: evidence, mechanisms, and perspectives. Biochar 6(1):42773. https://doi.org/10.1007/s42773-024-00308-3
29. Hu L, Cao LX, Zhang RD (2014) Bacterial and fungal taxon changes in soil microbial community composition induced by short-term biochar amendment in red oxidized loam soil. World J Microbiol Biotechnol 30:1085–1092. https://doi.org/10.1007/s11274-013-1528-5
30. Hu N, Lang T, Ding D, Hu J, Li C, Zhang H et al (2019) Enhancement of repeated applications of chelates on phytoremediation of uranium contaminated soil by *Macleaya cordata*. J Environ Radioact 199:58–65. https://doi.org/10.1016/j.jenvrad.2018.12.023
31. Hu N, Xiao FF, Zhang DD, Hu RW, Xiong R, Lv WP et al (2024) Organophosphorus mineralizing-Streptomyces species underpins uranate immobilization and phosphorus availability in uranium tailings. J Hazard Mater 476:134975. https://doi.org/10.1016/j.jhazmat.2024.134975
32. Hussain B, Li JM, Ma YB, Chen Y, Wu CY, Ullah A et al (2021) A field evidence of Cd, Zn and Cu accumulation in soil and rice grains after long-term (27 years) application of swine and green manures in a paddy soil. Sustainability 13(4):2404. https://doi.org/10.3390/su13042404
33. Hu XM, Wang JL, Lv Y, Liu XY, Zhong J, Cui XL et al (2021) Effects of heavy metals/metalloids and soil properties on microbial communities in farmland in the vicinity of a metals smelter. Front Microbiol 12:2347. https://doi.org/10.3389/fmicb.2021.707786
34. Hu Z, Zhao C, Li Q, Feng Y, Zhang X, Lu Y et al (2023) Heavy metals can affect plant morphology and limit plant growth and photosynthesis processes. Agronomy 13(10):2601. https://doi.org/10.3390/agronomy13102601
35. Islam W, Zeng FJ, Alotaibi MO, Khan KA (2024) Unlocking the potential of soil microbes for sustainable desertification management. Earth-Sci Rev 252:104738. https://doi.org/10.1016/j.earscirev.2024.104738
36. Johnston ER, Hatt JK, He ZL, Wu LY, Guo X, Luo YQ et al (2019) Responses of tundra soil microbial communities to half a decade of experimental warming at two critical depths. Proc Nati Acad Sci 116(30):15096–15105. https://doi.org/10.1073/pnas.1901307116
37. Jun BM, Chae SH, Kim D, Son C, Kim TJ, Hong SW et al (2025) Remediation of acidic effluents from uranium-contaminated soil using coffee residue biochar: a combined experimental and machine learning approach. Sep Purif Technol 366:132844. https://doi.org/10.1016/j.seppur.2025.132844
38. Kang DD, Li F, Kirton E, Thomas A, Egan R, An H et al (2019) MetaBAT 2: an adaptive binning algorithm for robust and efficient genome reconstruction from metagenome assemblies. PeerJ 7:e7359. https://doi.org/10.7717/peerj.7359
39. Kasko J, Li X, Müller K, Ge Y, Vettese GF, Law GTW et al (2023) Uranium (VI) interactions with *Pseudomonas* sp. PS-0-L, V4-5-SB and T5-6-I. Appl Geochem 159:105829.

https://doi.org/10.1016/j.apgeochem.2023.105829

40. Kolhi ML, Hussain A, Junejo AR, Zhang LW, Gu YC, Zhu YY et al (2026) Mechanistic insights into heavy metals detoxification and signaling in plants: Molecular coordination and stress tolerance an updated overview. Plant Stress 20:101284. https://doi.org/10.1016/j.stress.2026.101284
41. Kudpeng K, Khoiri AN, Duangfoo T, Cheevadhanarak S, Jirakkakul J (2025) Microbial–organic inputs with glycine supplementation enhance growth and heat stress tolerance in lettuce. Horticulturae 11(8):935. https://doi.org/10.3390/horticulturae11080935
42. Liao J, Ding L, Zhang Y, Zhu W (2022) Efficient removal of uranium from wastewater using pig manure biochar: understanding adsorption and binding mechanisms. J Hazard Mater 423:127190. https://doi.org/10.1016/j.jhazm at. 2021. 127190
43. Liu H, Du X, Li Y, Han X, Li B, Zhang X et al (2022) Organic substitutions improve soil quality and maize yield through increasing soil microbial diversity. J Clean Prod 347:131323. https://doi.org/10.1016/j.jclepro.2022.131323
44. Liu T, Liu L, Zhou TS, Chen YK, Zhou H, Liu J et al (2025) Chalcone isomerase gene (OsCHI3) increases rice drought tolerance by scavenging ROS via flavonoid and ABA metabolic pathways. Crop J 13(2):372–384. https://doi.org/10.1016/j.cj.2025.01.019
45. Liu YR, Lan XJ, Hou HQ, Ji JH, Liu XM, Lv ZZ (2024) Multifaceted ability of organic fertilizers to improve crop productivity and abiotic stress tolerance: Review and perspectives. Agronomy 14(6):1141. https://doi.org/10.3390/agronomy14061141
46. Li W, Li J, Liu B, Yu R, Wang J, Chen L et al (2025) Electroreduction of U(VI) in nitric acid solution: Efficiency optimization and the impact of impurities. J Radioanal Nucl Chem 334(11):8169–8178. https://doi.org/10.1007/s10967-025-10517-0
47. Li XF, Basak B, Tanpure RS, Zheng X, Jeon BH (2025) Unraveling the genetic basis of microbial metal resistance: Shift from Mendelian to systems biology. J Hazard Mater 493:138350. https://doi.org/10.1016/j.jhazmat.2025.138350
48. Luo YJ, Veelen HPJV, Chen SY, Sechi V, Heijne A, Veeken A et al (2022) Effects of sterilization and maturity of compost on soil bacterial and fungal communities and wheat growth. Geoderma 409:115598. https://doi.org/10.1016/j.geoderma.2021.115598
49. Meliani A, Bensoltane A, Benidire L, Oufdou K (2017) Plant growth-promotion and IAA secretion with *Pseudomonas* fluorescens and *Pseudomonas* putida. Res Rev J Bot Sci 6(2):16–24
50. Mishra S, Xia SM, Wang WT, Yang XD (2026) Elevation, soil pH and calcium availability shape regional and local scale spatial patterns of *PhoD* gene abundance in tropical and subtropical forests. Funct Ecol 40(4):983–1000. https://doi.org/10.1111/1365-2435.70264
51. Misson J, Henner P, Morello M, Floriani M, Wu TD, Guerquin-Kern JL et al (2009) Use of phosphate to avoid uranium toxicity in Arabidopsis thaliana leads to alterations of morphological and physiological responses regulated by phosphate availability. Environ Exp Bot 67(2):353–362. https://doi.org/10.1016/j.envexpbot.2009.09.001

52. Muhammad I, Hu SL, Luo XG, Ying C, Naseem S (2024) Screening and signifying the uranium remediation level of *Alternanthera philoxeroides* and *Eichhornia crassipes* from aquatic medium. Environ Pollut 342:123063. https://doi.org/10.1016/j.envpol.2023.123063
53. Pentyala VB, Eapen S (2020) High efficiency phytoextraction of uranium using *Vetiveria zizanioides* L. Nash. Int J Phytoremediat 22(11):1137–1146. https://doi.org/10.1080/15226514.2020.1741506
54. Peters A, Nawrot TS, Baccarelli AA (2021) Hallmarks of environmental insults. Cell 184(6):1455–1468. https://doi.org/10.1016/j.cell.2021.01.043
55. Qian LS, Zakriya M, Pervez M, Waqar I, Song ZH, Younis U et al (2023) Assessing the synergistic effect of acidified carbon, inorganic fertilizer, and biofertilizer on fenugreek antioxidant levels, and quality traits. J King Saud Univ Sci 35(7):102848. https://doi.org/10.1016/j.jksus.2023.102848
56. Qi X, Xiao SQ, Chen XM, Ali I, Gou JL, Wang D et al (2022) Biochar-Based Microbial Agent Reduces U and Cd Accumulation in Vegetables and Improves Rhizosphere Microecology. Soc Sci Electron Publ 436:129147. https://doi.org/10.1016/j.jhazmat.2022.129147
57. Schloss PD, Westcott SL, Ryabin T, Hall JR, Hartmann M, Hollister EB et al (2009) Introducing mothur: open-source, platform-independent, community-supported software for describing and comparing microbial communities. Appl Environ Microbiol 75(23):7537–7541. https://doi.org/10.1128/AEM.01541-09
58. Suvendran S, Acevedo MF, Smithers B, Walker SJ, Xu P (2025) Soil fertility and plant growth enhancement through compost treatments under varied irrigation conditions. Agric Basel 15(7):734. https://doi.org/10.3390/agriculture15070734
59. Tan JL, Chen YX, Deng QW, Ding DX, Hu N, Han JY et al (2025) The decomposition process of uranium-accumulating plant litter: secondary release of uranium and its impact on soil microbial communities. J Radioanal Nucl Chem 334:6015–6027. https://doi.org/10.1007/s10967-025-10322-9
60. Tan WF, Deng ZW, Lv JW, Tang DS, Li JX, Peng C (2024) The Effect of bacteria on uranium sequestration stability by different forms of phosphorus. Environ Technol 46(6):922–930. https://doi.org/10.21203/rs.3.rs-3835686/v1
61. Trivedi P, Leach JE, Tringe SG, Sa T, Singh BK (2020) Plant–microbiome interactions: from community assembly to plant health. Nat Rev Microbiol 18(11):607–621. https://doi.org/10.1038/s41579-020-00490-8
62. Uritskiy GV, DiRuggiero J, Taylor J (2018) MetaWRAP—a flexible pipeline for genome-resolved metagenomic data analysis. Microbiome 6:158. https://doi.org/10.1186/s40168-018-0541-1
63. Wang HS, Guo R, Xu JL, Yang T, Wang MM, Zhang L et al (2025) Organic fertilizer enhances crop yield and soil health by increasing arbuscular mycorrhizal fungi species richness. Funct Ecol 39(11):3210–3224. https://doi.org/10.1111/1365-2435.70151
64. Wang XM, Ge QS, Geng X, Wang ZS, Gao L, Bryan BA et al (2023) Unintended consequences of combating desertification in China. Nat Commun 14:1139. https://doi.org/10.1038/s41467-023-36835-z

65. Wang XM, Wu M, Wei ZJ, Hazard CW, Nicol G, Zha HC et al (2024) Investigating drivers of free-living diazotroph activity in paddy soils across China. Soil Biol Biochem 199:109601. https://doi.org/10.1016/j.soilbio.2024.109601
66. Wu Y, Xie YH, Liu XL, Li Y, Wang JY, Chen ZS et al (2023) Functional nanomaterials for selective uranium recovery from seawater: material design, extraction properties and mechanisms. Coord Chem Rev 483:215097. https://doi.org/10.1016/j.ccr.2023.215097
67. Wu XY, Amanze C, Yu ZJ, Li JK, Liu YD, Shen L et al (2022a) Evaluation of fungal community assembly and function during food waste composting with *Aneurinibacillus* sp. LD3 inoculant. Bioresour Technol 363:127923. https://doi.org/10.1016/j.biortech.2022.127923
68. Wu XY, Amanze C, Yu RL, Li JK, Wu XL, Shen L et al (2022b) Insight into the microbial mechanisms for the improvement of composting efficiency driven by *Aneurinibacillus* sp. LD3. Bioresour Technol 359:127487. https://doi.org/10.1016/j.biortech.2022.127487
69. Xiao M, Jiang SG, Li JB, Li WP, Fu PX, Liu GM et al (2025) Synergistic effects of bio-organic fertilizer and different soil amendments on salt reduction, soil fertility, and yield enhancement in salt-affected coastal soils. Soil Tillage Res 248:106433. https://doi.org/10.1016/j.still.2024.106433
70. Xiong XN, Liu J, Xiao TF, Lin K, Huang YL, Deng PY et al (2025) Remediation of uranium-contaminated water and soil by biochar-based materials: a review. Biochar 7:41. https://doi.org/10.1007/s42773-025-00438-2
71. Yang HZ, Fan ST, Jiang MZ, Hu YD, Chen XY, Liu WS et al (2025) Biochar-organic fertilizer synergy drives microbial-mediated C-sequestration and N-cycling in mixed forests toward sustainability. J Environ Manage 392:126892. https://doi.org/10.1016/j.jenvman.2025.126892
72. Yang JK, Ren YN, Jia MK, Huang SM, Guo TF, Liu BY et al (2025) Improving soil quality and crop yield of fluvo-aquic soils through long-term organic-inorganic fertilizer combination: Promoting microbial community optimization and nutrient utilization. Environ Technol Innov 37:104050. https://doi.org/10.1016/j.eti.2025.104050
73. Yang X, Dai Z, Ge C, Yu HM, Bolan N, Tsang DCW et al (2023) Multiple-functionalized biochar affects rice yield and quality via regulating arsenic and lead redistribution and bacterial community structure in soils under different hydrological conditions. J Hazard Mater 443:130308. https://doi.org/10.1016/j.jhazmat.2022.130308
74. Yassine C, Marta SV, Hugo H, Idrissi MM, Carpin S, Bourgerie S et al (2025) Synergistic effects of compost and biochar on soil health and heavy metal stabilization in contaminated mine soils. Agronomy 15(6):1295. https://doi.org/10.3390/agronomy15061295
75. Yuan WH, She JY, Liu J, Zhang Q, Wei XD, Huang LT et al (2024) Insight into microbial functional genes' role in geochemical distribution and cycling of uranium: the evidence from covering soils of uranium tailings dam. J Hazard Mater 461:132630. https://doi.org/10.1016/j.jhazmat.2023.132630
76. Yu H, Liu SW, Zhang DD, Hu RW, Chen PB, Liu HP et al (2025) Specific enrichment of *arsM*-carrying microorganisms with nitrogen fixation and dissimilatory nitrate reduction function enhances arsenic

methylation in plant rhizosphere soil. Environ Sci Technol 59(3):1647–1660. https://doi.org/10.1021/acs.est.4c10242

77. Yu H, Lv WP, Ding DX, Hu N, Zhang H, Chen MF et al (2025) Arsenite-oxidizing chemolithooautotrophic prokaryotes underpin inorganic carbon fixation and arsenic detoxification in deep underground uranium mining layers. J Hazard Mater 496(15):139213. https://doi.org/10.1016/j.jhazmat.2025.139213
78. Yu H, Zhang DD, Xiong R, Liu SW, Hu RW, Chen PB et al (2025) Soil-dependent responses of bacterial communities, phosphorus and carbon turnover to uranium stress in different soil ecosystems. J Hazard Mater 493:391259. https://doi.org/10.1016/j.jhazmat.2025.138383
79. Yu J, Zhang BF, Chen JQ, Mao WH, Lou LP, Shen CF et al (2021) Biofertilizer-induced response to cadmium accumulation in *Oryza sativa* L. grains involving exogenous organic matter and soil bacterial community structure. Ecotox Environ Safe 211(15):111952. https://doi.org/10.1016/j.ecoenv.2021.111952
80. Zhang C, Xu H, Zhou X, Liu Y, Liu JB, Wang WX et al (2025) Progress in microbial remediation of uranium: Mechanistic investigations, environmental applications and impact analysis. J Environ Chem Eng 13(6):119769. https://doi.org/10.1016/j.jece.2025.119769
81. Zhang D, Li M, Yang Y, Yu H, Xiao F, Mao C et al (2022) Nitrite and nitrate reduction drive sediment microbial nitrogen cycling in a eutrophic lake. Water Res 220:118637. https://doi.org/10.1016/j.watres.2022.118637
82. Zhang Y, Fang Q, Lv JW, Fu YK, Zhu JH, Peng GJ et al (2023) Source control on the acid mine drainage produced by the oxidation of pyrite and sulfur-containing uranium tailings based on the microbially induced carbonate precipitation technology. J Clean Prod 428:139444. https://doi.org/10.1016/j.jclepro.2023.139444
83. Zhao JR, Liu ZJ, Zhai BN, Jin H, Xu XP, Zhu YJ (2023) Long-term changes in soil chemical properties with cropland-to-orchard conversion on the Loess Plateau, China: Regulatory factors and relations with apple yield. Agr Syst 204:103562. https://doi.org/10.1016/j.agsy.2022.103562
84. Zhao TC, He AB, Khan MN, Yin Q, Song SK, Nie LX (2024) Coupling of reduced inorganic fertilizer with plant-based organic fertilizer as a promising fertilizer management strategy for colored rice in tropical regions. J Integr Agric 23(1):93–107. https://doi.org/0.1016/j.jia.2023.04.035
85. Zhao XY, Dang QL, Wang Y, Zhang CY, Chen YT, He LZ et al (2023) Linking redox characteristics to dissolved organic matter derived from different biowaste composts: a theoretical modeling approach based on FT–ICR MS analysis. Environ Sci Technol 40:57. https://doi.org/10.1021/acs.est.3c03286
86. Zheng SJ, Guo D, Yang XY, Liu Y, Tian SH, Tian WW et al (2025) Full life cycle of uranium toward ore-soil-root-shoot system: a comprehensive review. Crit Rev Env Sci Tec 55(2):2386104. https://doi.org/10.1080/10643389.2024.2386104
87. Zhu KJ, Yang ZL, Li MC, Deng QW, Xiao FF, Wang YD et al (2026) Synergistic enhancement of phytoremediation efficiency and mechanisms of uranium-contaminated soil by oxalic acid and

endophytic fungus *Fusarium* sp. A-2 with *Macleaya cordata*. J Environ Radioactiv 291:107844. https://doi.org/10.1016/j.jenvrad.2025.107844

88. Zhu L, Jia X, Li MX, Wang Y, Zhang JP, Hou JQ et al (2021) Associative effectiveness of bio-organic fertilizer and soil conditioners derived from the fermentation of food waste applied to greenhouse saline soil in Shan Dong Province, China. Appl Soil Ecol 167:105006. https://doi.org/10.1016/j.apsoil.2021.104006

Figures

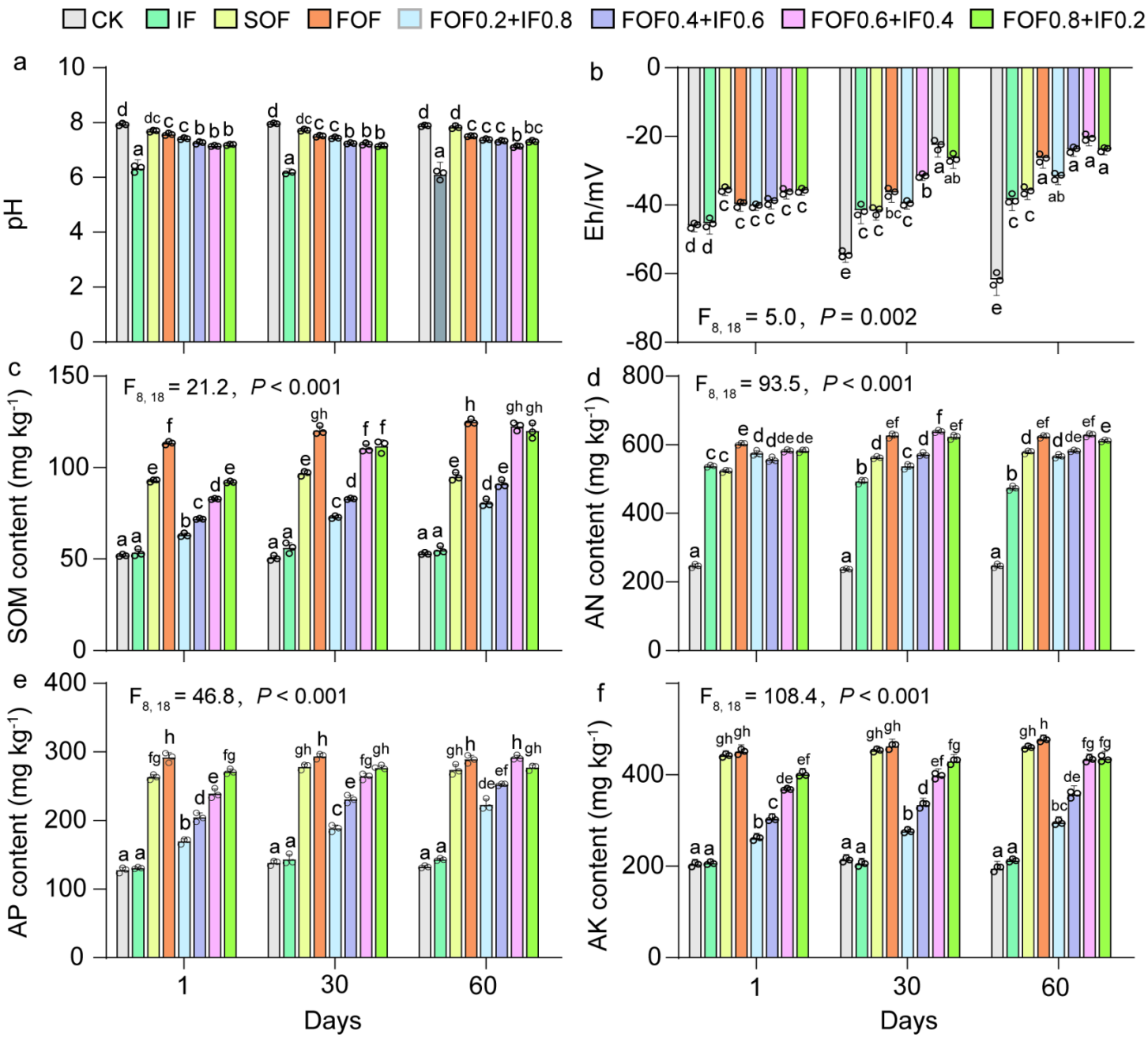

Figure 1

Temporal dynamics of soil physicochemical factors under the treatment of different proportions of organic fertilizers and inorganic fertilizers. Changes in (a) pH, (b) Eh, the content of (c) soil organic matter (SOM), (d) available nitrogen (AN), (e) available phosphorus (AP), and (f) available potassium (AK). CK, no fertilizer. IF, 100% inorganic fertilizer. SOF, 100% sheep manure organic fertilizer. FOF, 100% food waste-derived organic fertilizer. $FOF_{0.2}$+$IF_{0.8}$, 20% inorganic fertilizer substitution with FOF. $FOF_{0.4}$+$IF_{0.6}$, 40% inorganic fertilizer substitution with FOF. $FOF_{0.6}$+$IF_{0.4}$, 60% inorganic fertilizer substitution with FOF. $FOF_{0.8}$+$IF_{0.2}$, 80% inorganic fertilizer substitution with FOF. The different lowercase letters indicate significant differences on the level of $P < 0.05$ using two-way ANOVA (n = 3).

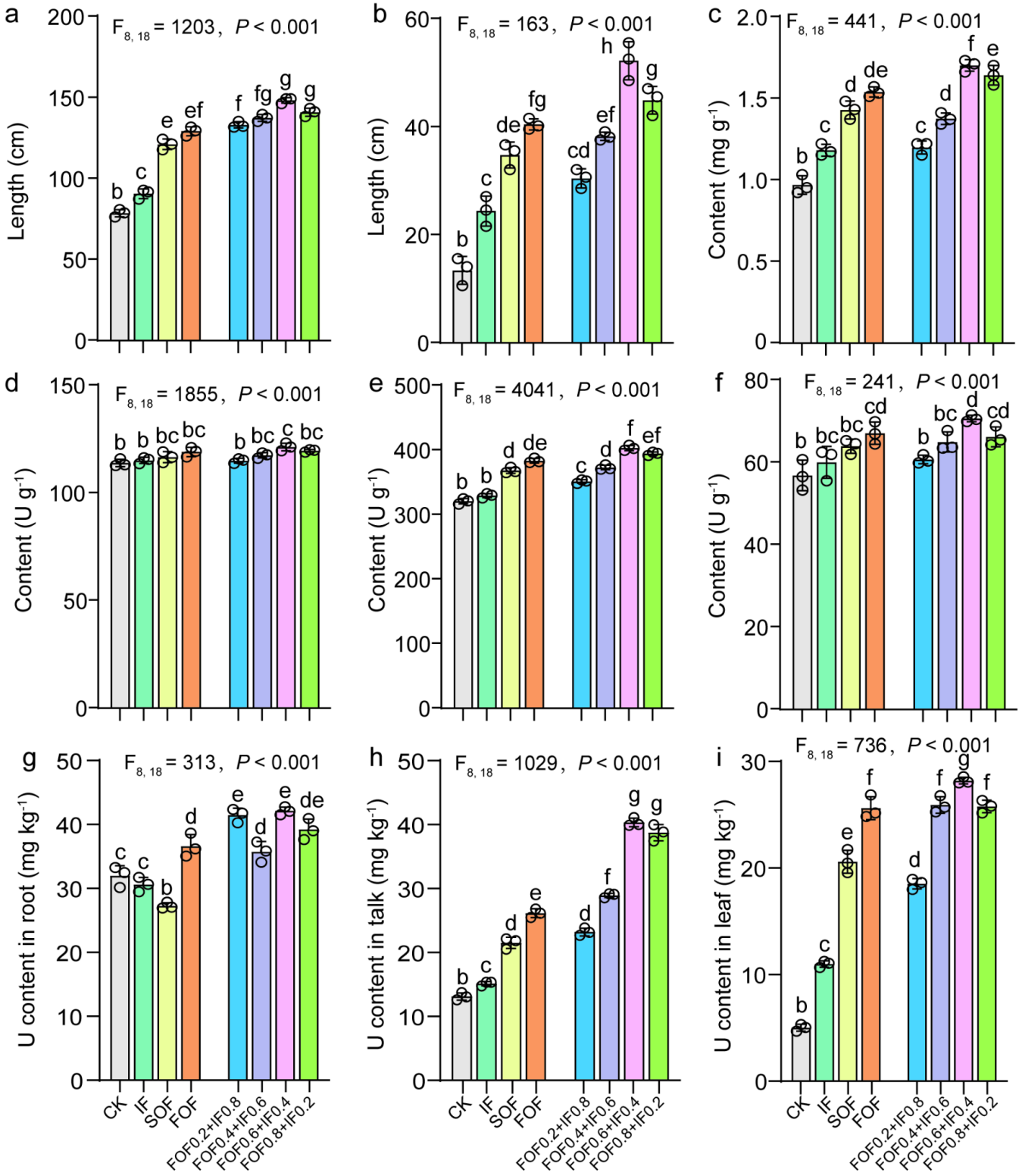

Figure 2

Comparison of the plant parameters and uranium content under the treatment of different proportions of organic fertilizers and inorganic fertilizers. (a) Shoot length. (b) Root length. (c) Total chlorophyll content in leaves. (d) Superoxide Dismutase (SOD) activity in leaves. (e) Peroxidase (POD) activity in leaves. (f) Catalase (CAT) activity in leaves. (g) Uranium content in root. (h) Uranium content in talk. (i) Uranium

content in leaves. The different lowercase letters indicate significant differences on the level of $P < 0.05$ using two-way ANOVA (n = 3).

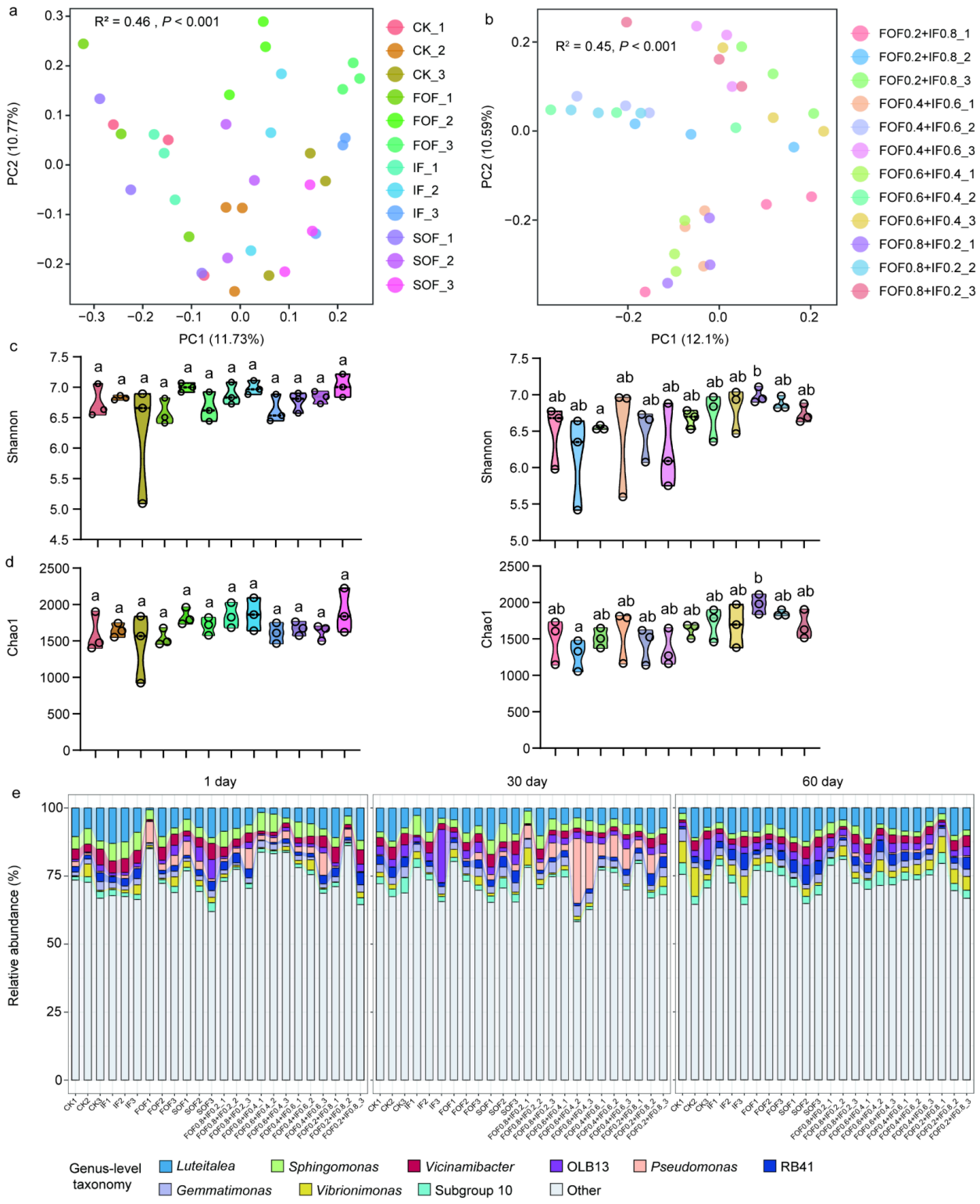

Figure 3

Diversity and dynamic composition analysis of bacteria communities in the rhizosphere of *V. zizanioides*. Principal coordinate analysis (PCoA) of the microbial communities among CK, IF, SOF, and FOF

treatments (a) and under different proportions of combined IF and FOF application (b). In both panels, the suffixes _1, _2, and _3 denote samples collected on days 1, 30, and 60, respectively. Shannon (c) and Chao1 (d) diversity indices of bacterial communities under different fertilization treatments and combined application ratios, respectively. (e) Composition of bacterial communities at the genus level.

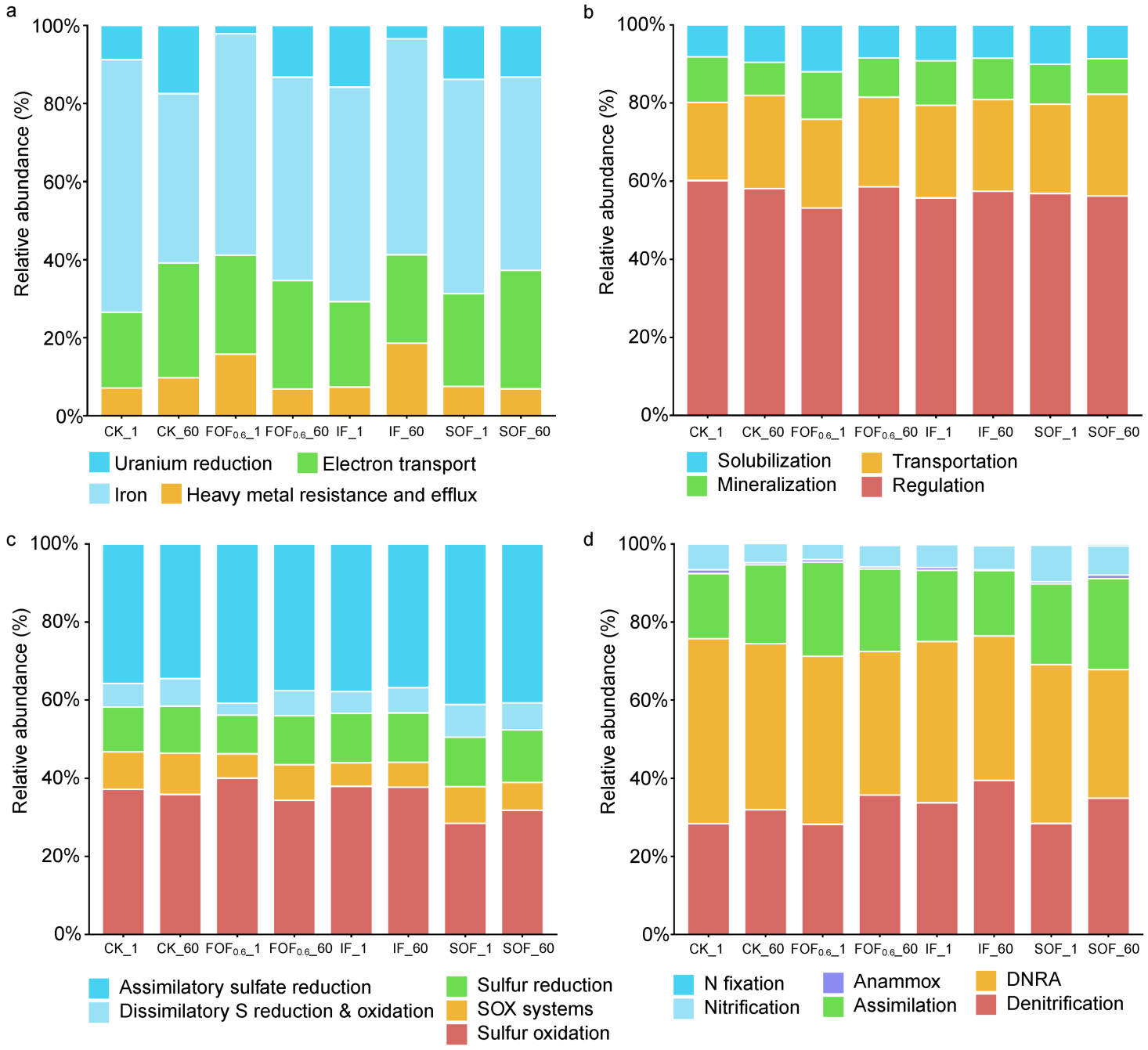

Figure 4

Change in the relative abundance of genes involved in heavy metal (a), P (b), S (c), and N (d) cycling under the treatment of organic fertilizers and inorganic fertilizers. $FOF_{0.6}$, 60% inorganic fertilizer substitution with FOF. DNRA, dissimilatory Nitrate Reduction to Ammonium.

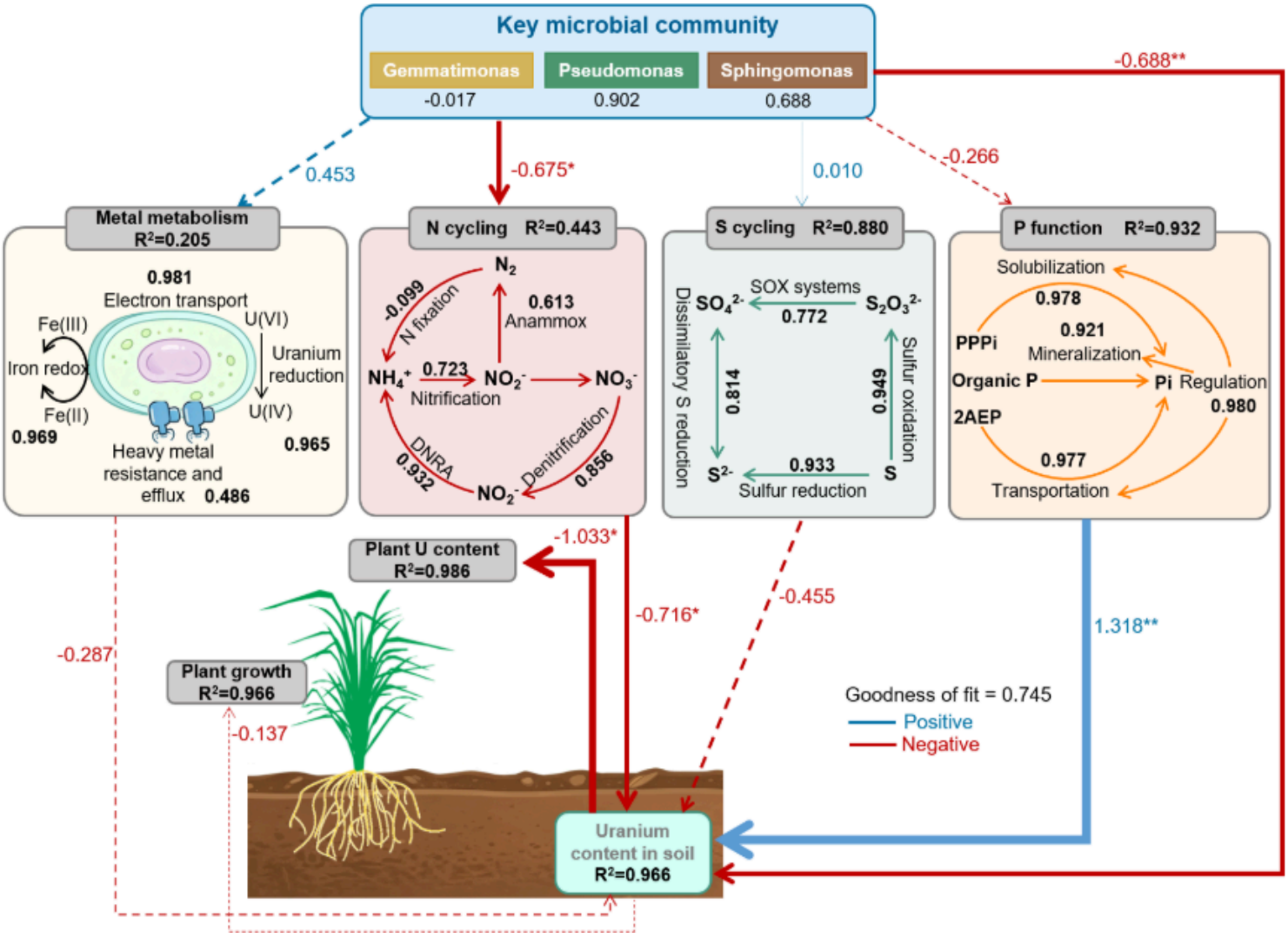

Figure 5

Path diagrams illustrating the links between key microbial communities, biogeochemical cycling, and uranium (U) fate. Blue and red arrows indicate positive and negative correlations, respectively. The numbers adjacent to the arrows represent standardized path coefficients, and the R^2 values within the boxes show the proportion of variance explained for each response variable. Single headed arrows refer to unidirectional causal relationships (*$P < 0.05$; **$P < 0.01$).

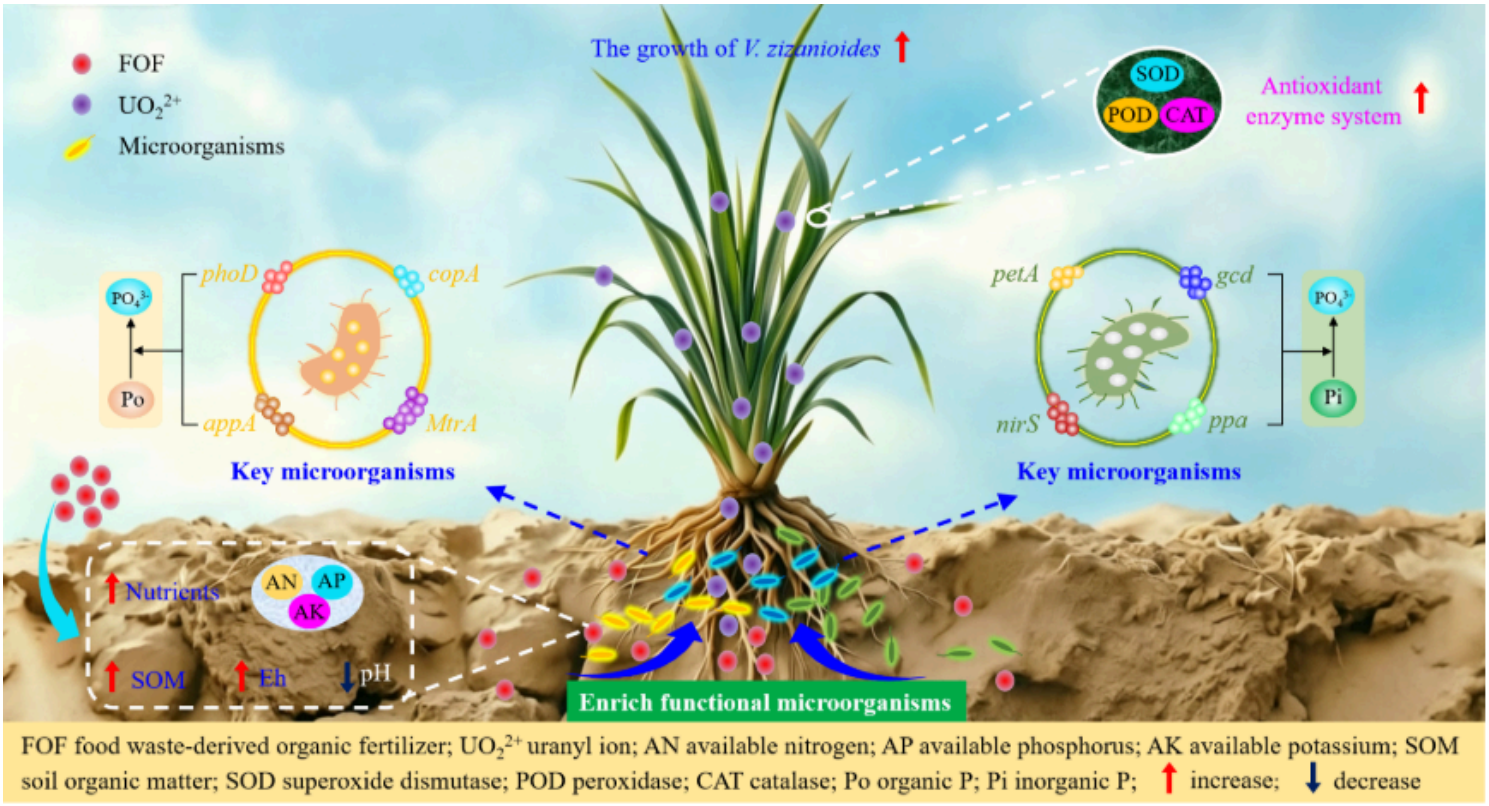

Figure 6

Schematic diagram of FOF-driven uranium phytoextraction by *V. zizanioides*.

Supplementary Files

This is a list of supplementary files associated with this preprint. Click to download.

- SupplementaryMaterial1117.docx